Int. J. Electrochem. Sci., 17 **(2022)** Article Number: 220849, doi: 10.20964/2022.08.49

International Journal of
ELECTROCHEMICAL
SCIENCE
www.electrochemsci.org

Effects of Electrochemical Chloride Extraction on the Properties of Chloride-Contaminated Reinforced Concrete by Using Magnesium Phosphate Cement Bonding Carbon Fiber Reinforced Plastics as Anode

Yue Li, and Hui Lin[*]

The Key Laboratory of Urban Security and Disaster Engineering, MOE. Beijing University of Technology, 100124, China
[*]E-mail: lin52hui90@126.com

Received: 7 April 2022 / *Accepted:* 15 May 2022 / *Published:* 4 July 2022

This paper adopts magnesium phosphate cement (MPC) bonding carbon fiber reinforced plastics (CFRP) as anode and mainly studies the influences of electrochemical chloride extraction (ECE) on the ions distribution, mechanical properties and pore structure of reinforced concrete under varying current densities and temperatures. Results show that the ECE efficiency is mainly affected by the factor of current density. ECE results in the re-distribution of ions in concrete. The increase in current density results in an obvious reduction of Cl^- and the increases of OH^-, K^+, Na^+ and Ca/Si ratio in the regions nearby rebar. Meanwhile, from rebar surface to concrete surface, Cl^- shows an increasing trend and OH^-, K^+, Na^+ and Ca/Si ratio present a decreasing trend. ECE treatment can significantly reduce the corrosion risk of rebar by the excellent Cl^- removal efficiency. However, the decrease in small pore and the increase in large pore result in the deterioration of concrete mechanical properties after ECE treatment. Comprehensively consider the influences of ECE on chloride removal efficiency, bonding strength retention and compressive strength retention by using efficacy coefficient analysis, the optimal current density and temperature for ECE are $2A/m^2$ and 35°C.

Keywords: Electrochemical Chloride Extraction; Corrosion risk; Magnesium Phosphate Cement;

1. INTRODUCTION

Corrosion of rebar is the primary threat to the durability of concrete structures. Sufficient Cl^- can disrupt the rebar surface passive film resulting in the deterioration of concrete [1, 2]. Various methods, such as surface coating, impregnation, using rust inhibitor are in the application for the protective of new-built concrete structure [3-5]. However, these processing methods only delay the corrosion time of rebar, which cannot completely eliminate the rebar corrosion. Furthermore, for the

corroded structures, which is usually repaired by cement mortar after eliminating the old concrete and the surface rust of rebar. This method is not a durable solution due to the rebar will be re-corroded by the diffusion of residue chloride ions [6].

Currently, cathodic protection (CP) and electrochemical chloride extraction (ECE) are two electrochemical protection methods for Cl^- polluted reinforced concrete [7-10]. However, CP operates in the whole service life of the structure with a relatively high current density (2-20mA/m^2), which is usually used in the marine reinforced concrete [11, 12]. Compared with CP, ECE requires a relative low current density and the treatment time is only several weeks [9, 13].

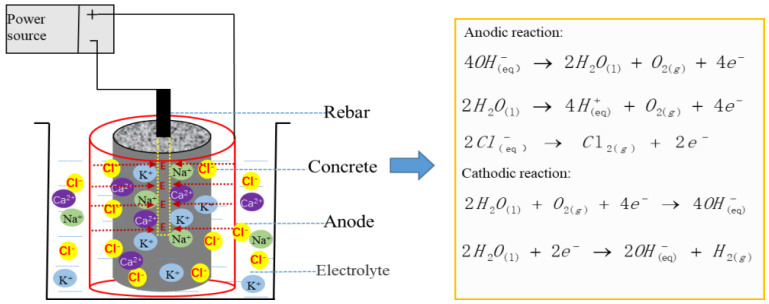

(a) ECE device (b) Reaction equations

Figure 1. The principle of ECE.

ECE process is usually handled in alkaline environment, during which rebar is regarded as cathode, and an extra anode is placed around concrete surface. The chemical reactions occur between anode and cathode are described as **Fig. 1**. Under the force of electric field, Cl^- removes from concrete, thereby reducing the corrosion risk of rebar [14].

Although ECE efficiency was affected by many factors including current density [15-17], water-cement ratio [18, 19], environment temperature [20-22], types of electrode and electrolyte [23-29], arrangement of steel reinforcement [30], cement type [31, 32], thickness of the reinforcement cover [15, 17, 24], previous studies implied that ECE could remove 30-80% chloride content after 6-10weeks treatment [23, 25, 32-33]. However, during ECE process, the electrochemical reaction and the migration and redistribution of ions changed the internal composition of concrete resulting in the deterioration of concrete properties [34-37]. Therefore, definiteness of ions redistribution after ECE treatment has great significance on the improvement of concrete properties [38].

Regarding this issue, M. Castellote [39] stated that chloride ion presented normal distribution in concrete after ECE treatment. R.N. Swamy [40] reported that the Cl^- content of concrete beam was high in middle cross section and was low in the region nearby rebar. Hu [11] found that the residual Cl^- first increased and then decreased from rebar surface to concrete surface. However, Jin [24] stated that chloride ion presented an increasing trend from inside to outside after ECE. Cañón [41] reported that ECE reduced the content of Cl^-, but the distribution rule of Cl^- was not obvious in concrete. For other ions, G. Fajardo [17] stated that the distribution of Na^+ and K^+ were mainly related to the thickness of

concrete cover. Liu [29] found that Na^+ and OH^- were distributed nearby the rebar region and K^+ was mainly enriched between cathode and anode. However, some simulation results reported that the concentration of Na^+, K^+ and OH^- presented a decreasing trend from rebar to concrete surface [42-44].

Our previous researches have affirmed the ECE effects by using magnesium phosphate cement (MPC) bond carbon fiber reinforced plastics (CFRP) as anode, and mainly focuses on the interfacial properties of rebar and concrete after ECE treatment, as well as the influences of ECE on the properties of corroded reinforced concrete [45, 46]. For comprehensive studying the understanding the evolution of concrete properties after ECE, this research aims to:

(1) Reveal the ions distribution in concrete after ECE treatment.

(2) Study the effects of ECE on the aperture evolution of concrete.

(3) Determine the appropriate parameters of applied current density and temperature with comprehensive consideration of chloride removal efficiency, bonding strength retention and compressive strength retention by using efficacy coefficient analysis.

To obtain that, the chloride-contaminated reinforced concrete was ECE treated 28 days with varying current densities (1A/m^2, 2A/m^2 and 3A/m^2) and temperature (15℃, 25℃ and 35℃) in the electrolyte of $Ca(OH)_2$. After that, the extraction efficiency of Cl^-, distribution of potassium, sodium and OH^- ions, Ca/Si ratios, mechanical properties and aperture evolution of the concrete were investigated.

2. EXPERIMENTAL DESCRIPTION

2.1. Raw materials

The chemical compositions and physical properties of the used dead burned MgO (calcined at 1600℃) and cement (P.O42.5) are presented in Table 1 and Table 2, respectively. The used coarse aggregate is continuously graded crushed stone (5~25mm). Siliceous river sand with the fineness modulus of 2.80 is used as fine aggregate. Polycarboxylate superplasticizer with the water reduction rate of 31% is used for concrete preparation. Tap water and deionized water are used for the preparation of concrete specimen and electrolytic solution, respectively. The purities of the used chemical purity reagents including KH_2PO_4, $Na_2B_4O_7{\cdot}10H_2O$, NaCl and $Ca(OH)_2$ are over 99%. The diameter of the used round carbon steel (Q235) bar is 10mm.

Table 1. Parameters of MgO

MgO (%)	CaO (%)	SiO_2 (%)	Al_2O_3 (%)	Fe_2O_3 (%)	Density (g/cm^3)	Bulk density(g/cm^3)	Specific surface area(cm^2/g)
91.7	1.4	1.6	4.0	1.3	3.46	1.67	805.9

The morphology of the used CFRP is shown in **Fig. 2,** which has a thickness and surface density of 0.19mm and 300g/m^2. The elastic modulus, fracture strain and ultimate tensile strength of CFRP are 210GPa, 0.02 and 4200MPa, respectively.

Table 2. Parameters of cement

Chemical composition (wt%)							Physical properties	
Loss	SiO_2	Fe_2O_3	Al_2O_3	CaO	MgO	SO_3	Specific gravity (g/cm^3)	Specific surface area (m^2/kg)
2.12	22.9	3.8	5.7	63.5	2.2	1.9	3.16	354

Figure 2. The morphology of CFRP.

2.2. Proportioning design

2.2.1. MPC

The proportioning and physical properties of the used MPC are shown in Table 3.

Table 3. Proportioning and properties of MPC [47-49]

P/M	B	W/C	Compressive strength(MPa)				Porosity (%)	Bonding strength with C30 concrete at 28days
			3h	1d	7d	28d		
1/4.5	5%	0.14	>20	>30	>40	>60	15~18	broken in concrete matrix

2.2.2. Concrete

The proportioning and properties of concrete are shown in Table 4. The addition of NaCl is 3wt%, and the Cl^-content is 1.82% of cement mass.

Table 4. Proportioning and properties of concrete

Cement (kg/m^3)	Aggregate (kg/m^3)	Sand (kg/m^3)	W/C ratio	Water Reduce (kg/m^3)	NaCl (kg/m^3)	compressive strength of 28 days (MPa)
325	1228	662	0.57	0.65	9.75	34.2

2.3. Experimental design

2.3.1. Concrete specimens preparation

The well-mixed concrete was poured into the size of Ø100×200mm PVC mold. The rebar with the length of 250mm was embedded in the central of the samples with an embedding depth of 150mm. After cured 24 hours, the specimens were demolded and masked the exposed rebar with epoxy resin to prevent corrosion. Subsequently, the samples were wrapped by MPC-CFRP. In the wrapping process, double-faced adhesive tape with the thickness and width of 5mm was adhered on CFRP to guarantee the thickness of MPC slurry was same. Then applied MPC slurry to CFRP and scraped the excess MPC paste along double-sided adhesive tape. Finally, rolling the concrete sample on MPC slurry until it was completely wrapped and the effective lap length of CFRP was set as 78.5mm (**Fig. 3**). After cured 28 days, the specimens were treated by ECE.

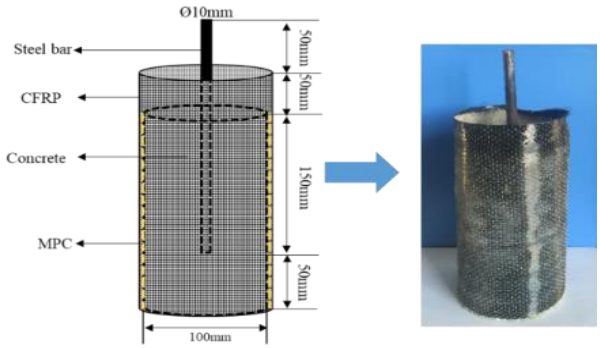

Figure 3. Concrete sample.

2.3.2. ECE treatment

Table 5. The parameters of ECE

Sample types	Sample No.	Current density(A/m^2)	ECE temperature (℃)
Control samples	C0T15	0	15
	C0T25	0	25
	C0T35	0	35
ECE treated samples	C1T15	1	15
	C2T15	2	15
	C3T15	3	15
	C1T25	1	25
	C2T25	2	25
	C3T25	3	25
	C1T35	1	35
	C2T35	2	35
	C3T35	3	35

Note: The control samples were soaked in the electrolyte with the temperature of 15℃, 25℃ and 35℃ without applying current, respectively. The ECE treated samples were applied the current densities of 1~3A/m^2 at the temperature of 15~35℃, respectively.

During ECE process, rebar and MPC-CFRP were the cathode and anode, respectively. The electrolyte was renewed every 2 days to prevent the overflow of chlorine and sampled to test the concentration of Cl^-. A heating rod was placed in the electrolyte to regulate and control the temperature (15℃, 25℃ and 35℃). The cling film was covered on the opening of the container to prevent the evaporation of electrolyte. A DC regulated power supply (HY3005ET, 0~30VDC, 0~5ADC, current resolution: 1mA) was contacted with cathode and anode to control the applied current densities(1A/m^2, 2A/m^2 and 3A/m^2) to concrete samples during 28 days. The ECE parameters and the schematic diagram of ECE device are presented in Table 5 and **Fig. 4**, respectively.

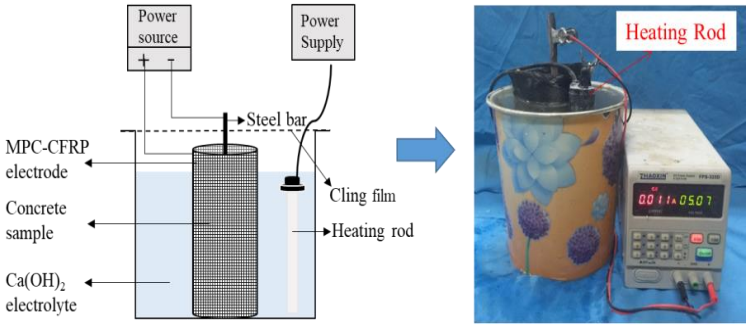

Figure 4. ECE device.

2.3.3 Axial compressive test

After ECE treatment, cutting the exposed rebar and polishing the concrete surface to smooth. The maximum axial compressive was tested by universal testing machine with the load rate of 0.5MPa/s. Three samples were tested in each groups and the compressive strength was obtained according to Eq. (1).

$$f_{max} = \frac{F_{max}}{A} \quad (1)$$

where, f_{max} is the maximum axial compressive strength of the sample. F_{max} is the maximum loading force. A is the cross-sectional area of the sample.

2.3.4 Ions distribution

After ECE for 28 days, the selected test area of the specimen was cut into slices with a thickness of 10mm **(Fig. 5(b)**). Subsequently, the slice was cut into four parts (site1~site4) along the diameter direction with the length of 12.5mm (**Fig. 5(c)**). Before grinding to mortar powder the concrete block was crushed and removing the stone. The obtained powder was mixed with deionized water at a mass ratio of 1:10 and stirred for 1 hours by heated magnetic stirrer, and filtered after placing for 24 hours. After centrifugation, the supernatant was used to test the concentrations of Cl^-, K^+ and Na^+ by ion chromatograph (C440, Velocity range: 0.001~10ml/min, detection range: 0~15000μS, resolution: 0.0047nS/cm). The content of Cl^- in different sites of concrete was calculated by Eq. (2).

$$\alpha = \frac{C_{Cl^-} \times V_0}{M \times W} \times 100\% \qquad (2)$$

where, C_{Cl^-} is the concentration of chloride ion in supernatant. V_0 is the volume of deionized water (50ml). M is the powder mass. W is the proportion of cement in powder.

pH meter (PAL-BX/ACID1) was used to test the pH of supernatant, and the OH^- concentration of the supernatant was calculated by Eq. (3).

$$C_{OH^-} = 10^{(pH-14)} \qquad (3)$$

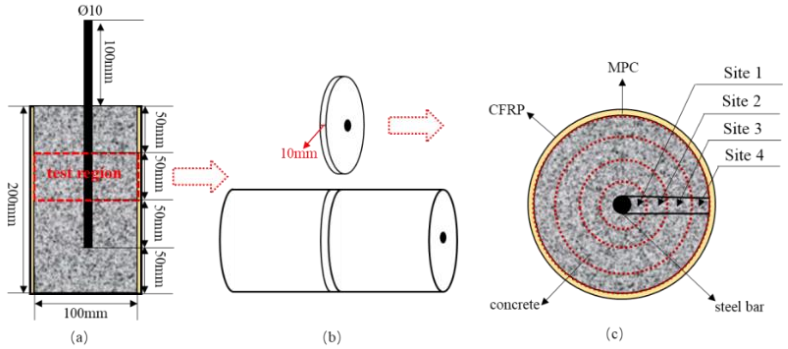

Figure 5. Sampling schematic diagram. (a) Concrete sample. (b) Slice cutting. (c) A slice.

After embedded the concrete block in epoxy resin (**Fig. 6)**, which was polished by the SiC paper with the size of 400, 800 and 1200. The Ca/Si ratios of site1~site4 were measured by scanning electron microscope (NOVA Nano SEM230) equipped with an energy dispersive spectrometer (EDS) in backscattered electron (BSE) mode. During the test, ten points were selected in each site. The obtained Ca/Si ratios were the average of the test results.

Figure 6. The sample used for Ca/Si ratio test.

2.3.5 Microstructure analysis

As shown in **Fig. 7**, concrete block with rebar in center (**Fig. 7 (b)**) was cut from the slice. Then, the block was polished by SiC paper with the size of 400, 800, 1200. The interfacial properties of rebar-concrete were observed by scanning electron microscope (NOVA Nano SEM230) equipped with an energy dispersive spectrometer (EDS) in backscattered electron (BSE) mode. During the test,

three points were selected in each region. The obtained element content was the average of the three points.

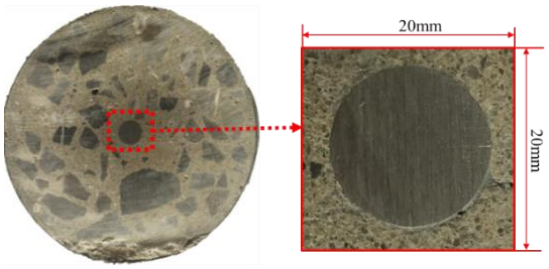

（a） （b）

Figure 7. Sampling schematic diagram. (a) Sampling region, (b) Concrete block.

2.3.6 Aperture analysis

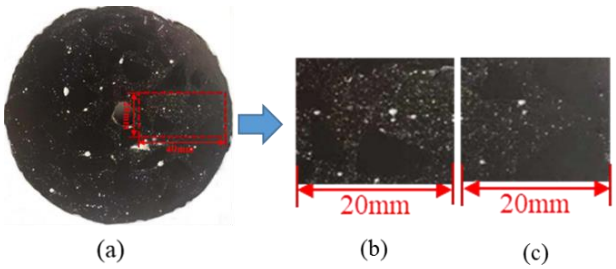

Figure 8. Diagram of test area for spacing coefficient of concrete bubbles.

After rebar was removed, the slice was sanded by SiC paper and polished by polishing machine. The surface of the slice was colored by ink and filled the bubbles by white nano powder (**Fig. 8(a)**). According to the Chinese standards of test code for hydraulic concrete (SL352-2006), the aperture of the concrete was measured. The results of the samples showed in **Fig. 8 (b)** and **(c)** were used to analysze the apertures in internal and external of the concrete, respectively.

3. RESULTS AND DISCUSSION

3.1 Chloride removal efficiency

The concentrations of Cl^- in electrolyte renewed at two-day intervals are presented in **Fig. 9**. **Fig. 9 (a)** shows that the concentration of Cl^- in electrolyte is close to 0 during 28 days at different temperatures when no current is applied to the sample. This phenomenon implies that the chloride ion in the control samples remains unchanged during the immersion period. After applying current density, the amount of the extracted chloride ion at two-day intervals presents a decreasing trend at varying temperatures with the extension of electric time. Furthermore, it can also find that the extraction amount of Cl^- at two-day intervals gradually increases with the increase of temperature at different

current densities during the first two weeks. As the electric time is prolonged (after two weeks), the Cl^- extraction amount at two-day intervals is relatively small and kept stable.

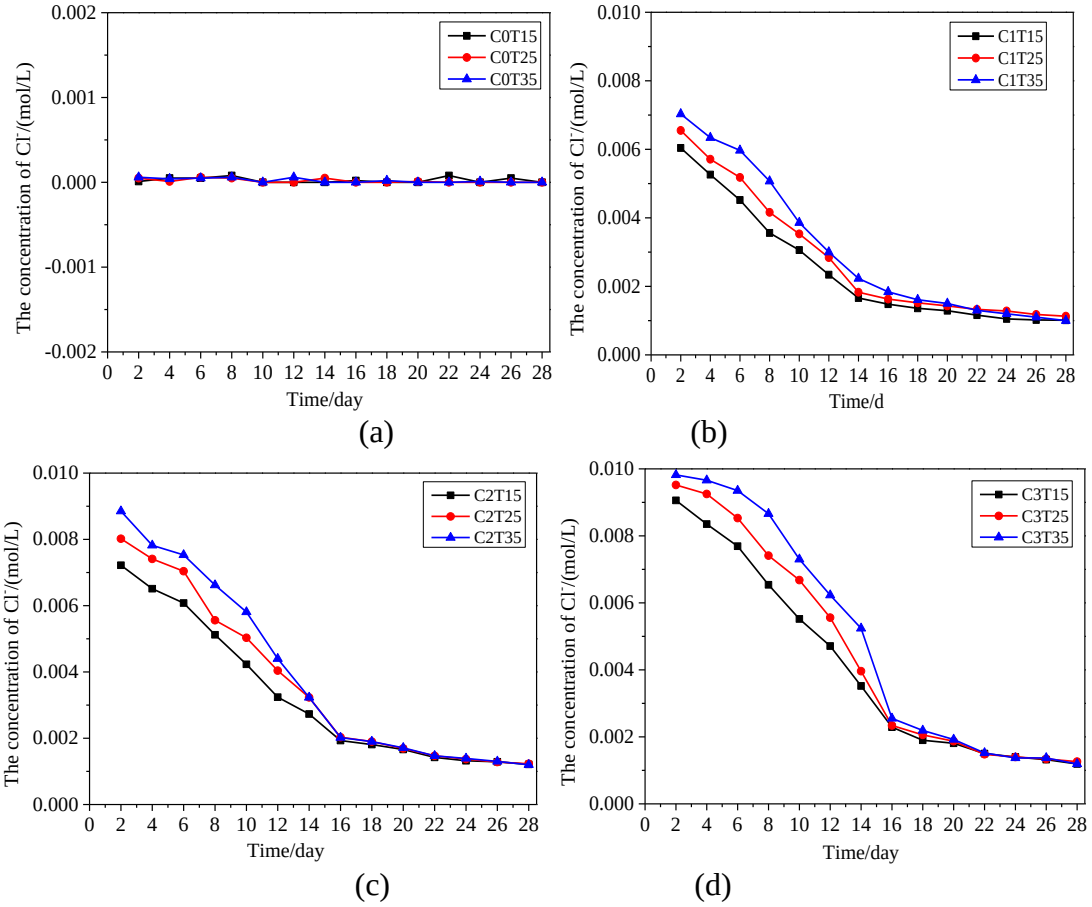

Figure 9. The Cl^-concentration in the electrolyte renewed at two-day intervals ((a) Control, (b) 1A/m^2, (c) 2A/m^2, (d) 3A/m^2).

The reasons for the results are as follows. Firstly, the directional movement and enrichment of the ions generate a reverse electric field between rebar and external anode, which weakens the driving force of the applied electric field for ions transmission, resulting in the reduction of chloride ions extraction amount. Secondly, the competitive transmission of cathodic reaction product (OH^-) for electron decreases the extraction amount of chlorine ion. Moreover, with the extension of extraction time, the amount of free chloride ion in concrete gradually decreases resulting in the extraction amount is small and keep stable.

According to Eq. (4) & (5), the cumulative chloride removal efficiency is obtained (**Fig. 10**).

$$M = V_S \times M_L \times W \quad (4)$$

$$Cl^-\% = \frac{M_{Cl^-} \times \sum C_i \times V_i}{M} \times 100\% \quad (5)$$

where, M is the initial content of Cl^- in concrete. V_s is sample volume. M_L is mass percentage of cement in concrete. W is mass proportion of Cl^- in cement. M_{Cl} is molar mass of Cl^-. C_i is the concentration of Cl^- in electrolyte at two-day intervals. V_i is the volume of renewed electrolyte.

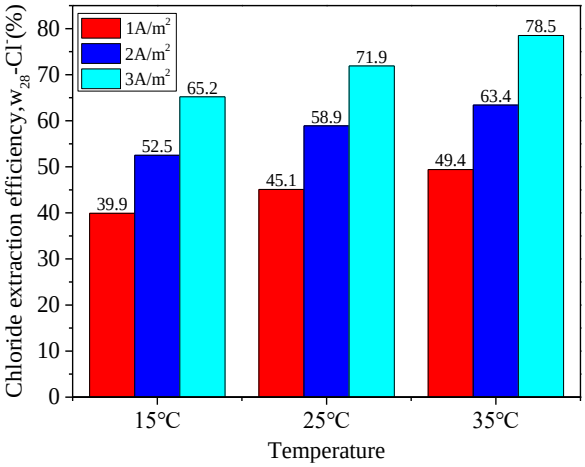

Figure 10. Cumulative chloride removal efficiency of concrete after 28 days.

Fig. 10 shows that the extraction efficiency of Cl^- increases with the increase in current density and temperature. The efficiency of MPC-CFRP is up to 78.5% at 3A/m^2 and 35℃, which is equivalent to the ECE efficiency of the widely used titanium mesh anode[23]. When operating at the same temperature, the efficiency increases by 25.3% at 15℃, 26.8% at 25℃ and 29.1% at 35℃ with the current density increase from 1A/m^2 to 3A/m^2, respectively. Furthermore, when the temperature increases from 15℃ to 35℃, the efficiency increases by 9.5%, 10.9% and 13.3% at the current densities of 1A/m^2, 2A/m^2 and 3A/m^2, respectively. Therefore, it is proposed that current density increases is the principal factor affecting the ECE efficiency. Temperature increases on the improvement of ECE efficiency is limited.

3.2 Ions distribution

3.2.1 Chloride ions

Fig. 11 presents the distribution and removal efficiency of Cl^- in different sites of concrete after ECE treated for 28 days. Results show that the residual Cl^- in concrete presents an increasing trend from site 1 to site 4 after ECE. As the temperature increases from 15℃ to 35℃, the Cl^- removal efficiency from site 1 to site 4 are 46.4%-20.0% (15℃), 50.0%-22.8% (25℃) and 52.5%-25.0% (35℃) at 1A/m^2, 59.6%-28.3% (15℃), 62.3%-30.0% (25℃) and 66.1%-34.4% (35℃) at 2A/m^2, 72.6%-38.2% (15℃), 75.4%-40.0% (25℃) and 78.1%-40.6% (35℃) at 3A/m^2, respectively. The results indicate that the content of Cl^- around rebar is significantly decreased with the increase in current density after ECE treatment by using the anode of MPC-CFRP, which has a similar Cl^- distribution in

comparison with the anode of CFRP, but the effect of MPC-CFRP anode has a better effect for the reduction degree of Cl^- content around rebar than CFRP, titanium mesh and conductive cement paste anodes [18, 23].

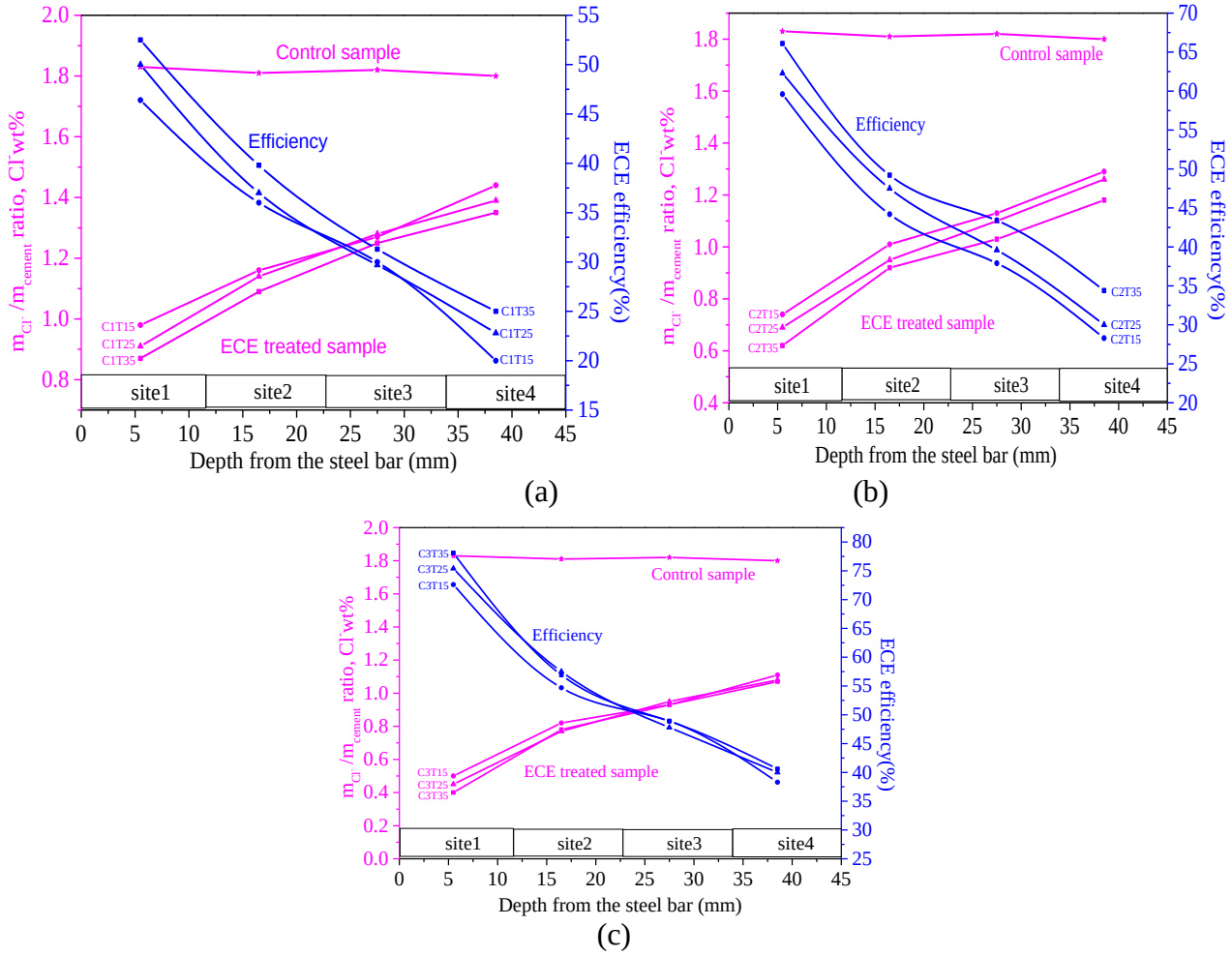

Figure 11. The distribution and removal efficiency of chloride ion in different sites of concrete : ((a) 1A/m^2, (b) 2A/m^2, (c) 3A/m^2).

To evaluate ECE on the protective effect of rebar, rebar-concrete interfacial morphology and composition are analyzed, as shown in **Fig. 12** (Here, taking the samples treated at 25℃ as example). It can be seen that the interfacial zone of samples C0T25 and C1T25 can be divided into three regions: rebar, concrete and rebar-concrete transition zone. EDS results indicate that the transition zone is the corrosion layer (T_{CL}), which is mainly comprised of rust and cement hydration products. For the control sample (C0T25), the rebar corrosion is relatively serious, the maximum T_{CL} width of which is up to 100.19μm after soaking 28 days. As the current densities increase to 2A/m^2 and 3A/m^2, the T_{CL} does not appear in the interfacial zone of samples C2T25 and C3T25, which implies that ECE can reduce the corrosion risk of rebar at a proper current density. However, the low Cl^- removal efficiency at the current density of 1A/m^2 results in the rebar in sample C1T25 is also corroded, but the corrosion

degree is greatly reduced for the decrease in T_{CL} width. The phenomenon was also observed by Saraswathy that the rebar also had potential corrosion risk when the current density of ECE was relative low [23].

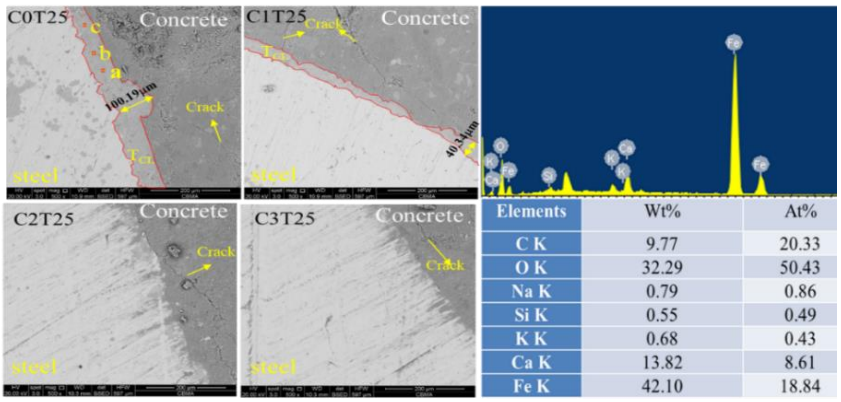

Elements	Wt%	At%
C K	9.77	20.33
O K	32.29	50.43
Na K	0.79	0.86
Si K	0.55	0.49
K K	0.68	0.43
Ca K	13.82	8.61
Fe K	42.10	18.84

(a)BSE analysis (b) EDS analysis

Figure 12. Analysis of rebar-concrete transition zone.

3.2.2 K^+, Na^+ and OH^-

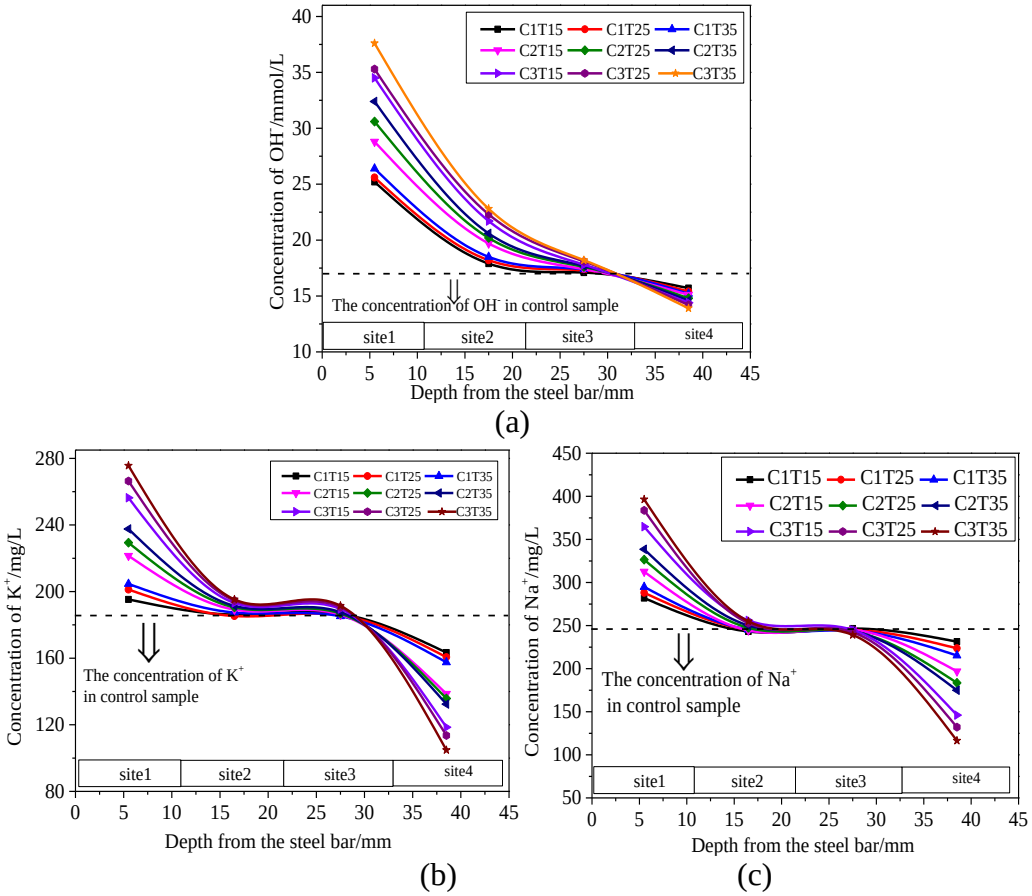

Figure 13. Distribution of K^+, Na^+ and OH^- in concrete: (a) OH^-, (b) K^+ and (c) Na^+.

The distributions of K^+, Na^+ and OH^- in concrete after ECE for 28 days are presented in **Fig. 13**. **Fig. 13 (a)** shows that the concentration of OH^- presents a decreasing trend from site1 to site 4. In comparison with control sample, the concentrations of OH^- in the samples after ECE treated are obviously changed, which are significantly increased nearby the rebar region (site 1) and are decreased in anode region (site 4) with the increasing current density and temperature. As presented in Fig. 1, cathodic reaction is a process of generating OH^-, which is the main reason for the increase in OH^- concentration nearby rebar region. Meanwhile, the increase in OH^- concentration in site 3 and site 4 is mainly due to the directional migration of OH^- by the driving force of electric field. However, anodic reaction is a process of consuming OH^-, thereby the concentration of OH^- in this region is decreased and is lower than that of the control sample.

Fig. 13 (b) and **(c)** present the distribution of K^+ and Na^+ in samples after ECE. Results show that the contents of K^+ and Na^+ in the samples are all present a decreasing trend from site 1 to site 4. The main reason is that the directional migration of cations by the force of electric field results in the enrichment of K^+ and Na^+ near the region of rebar (site 1), and the significantly decrease in the region of anode (site 4). Furthermore, compared with the influences of temperature, current density is the dominant reason affecting the redistributions of K^+ and Na^+. The higher current density results in the larger amount of cations enriching in the region nearby rebar.

The above result shows that ECE treatment will result in the enrichment of OH^-, K^+ and Na^+ in the region nearby rebar and the contents of these ions present an decreasing trend from inside to outside. These phenomena are also observed in the previous studies [42-44]. However, some other reports stated that the distribution rule of Cl^- was not obvious in concrete and the distribution of Na^+ and K^+ were mainly related to the thickness of concrete cover [17, 41]

3.2.3 Ca/Si ratio

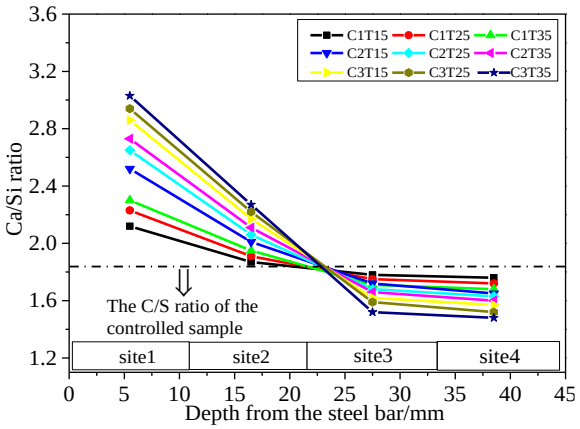

Figure 14. Ca/Si ratio in different sites of concrete after ECE treatment.

The Ca/Si ratio in different sites of the samples after ECE are presented in **Fig. 14**. Results show that the Ca/Si ratio also shows a decreasing trend from site 1 to site 4. The increase in current density and temperature result in the Ca/Si ratios in site 1 and site 2 increasing obviously in

comparison to control sample, which are up to 3.06 and 2.35 with the current density and temperature of 3A/m^2 and 35℃, respectively. While it is decreased in site 3 and site 4, and even lower than that of control sample. In comparison, the increase in current density is also the main reason for the variation of Ca/Si ratio after ECE. The changes may be associated with the following two processes: 1) the migration and enrichment of Ca^{2+} by the force of electric field lead to the increase in Ca/Si ratio of site 1 and site 2 ; 2) The directional migration of SiO_3^{2-} generated by the decomposition of C-S-H to anode region [45]. While some reports showed that the redistribution of Ca^{2+} was related to the thickness of concrete cover, and the maximum Ca^{2+} content was occurred in the depth of 16-24mm in the concrete when the thickness of rebar cover is 50mm [17].

3.3 Axial compressive strength

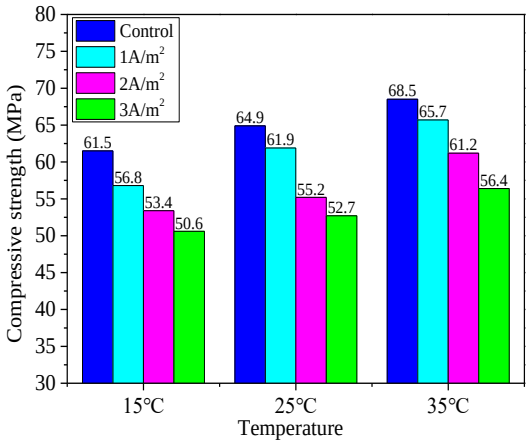

Figure 15. Axial compressive strength of concrete column after ECE treatment.

Fig. 15 shows the compressive strength of concrete after ECE treatment. It can be seen that the compressive strengths of ECE treated samples are all decreased with the increase in current density in comparison with control sample. While the increase in temperature is benefit to the strength development of concrete. As mentioned above, ECE treatment can cause the migration and redistribution of K^+, Na^+ and OH^-. The enrichment of these ions will soften the reaction productions of concrete and has negative effects on mechanical properties of the matrix [36-37, 45, 50]. Moreover, a higher current density usually results in a larger amount in decomposition of C-S-H [45]. Due to these reasons, the compressive strength of the sample is decreased in comparison with the control sample after ECE. However, In spite of this, the compressive strength of the sample after ECE by using the anode of MPC-CFRP is larger than the strength value of the designed concrete. The MPC-CFRP anode shows good reinforcement effect after ECE. While, some reports stated that ECE decreased the compressive strengths of concrete by using titanium mesh or steel wire mesh as anode [50]. And other studies indicated that ECE had no adverse effects on the compressive strength of concrete[40, 51].

3.4 Aperture analysis

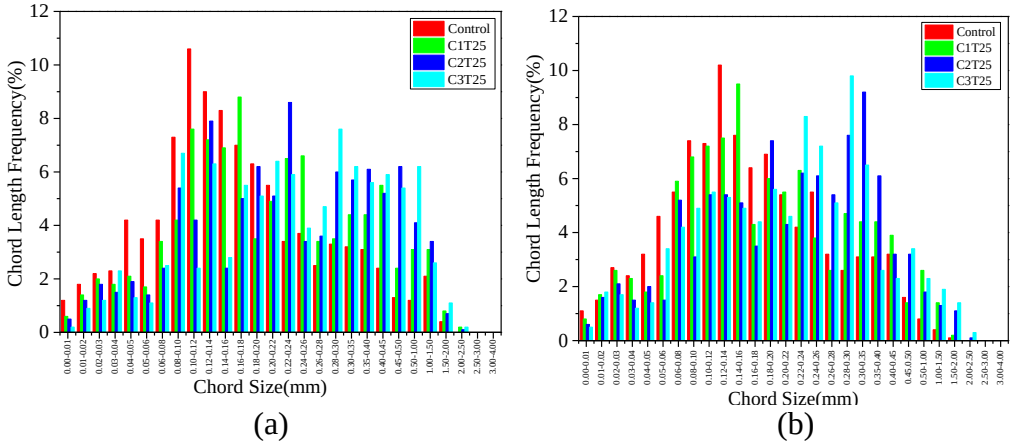

Figure 16. Chord length distribution: (a) internal chord length, (b) external chord length.

As abovementioned, current density is the primary factor that affects the efficiency of ECE. Therefore, this section mainly analyses the aperture of ECE samples treated at 25℃ and the chord length distribution in concrete is presented in **Fig. 16.**

Fig. 16 (a) is the distribution of chord length in internal concrete (sample Fig. 8(c)). Results shows that the frequency of the chord length distribution that less than 0.16mm is 54.6% in the control sample. As the current density increases, the frequencies of the chord length less than that 0.16mm presented a decreasing trend in ECE treated samples, which are 38.9% in C1T25, 30.6% in C2T25 and 27.7% in C3T25, respectively. While the frequencies of the chord length that larger than 0.18mm presents an increasing trend with the increase in current density, which are 61.1% at 1A/m^2, 69.4% at 2A/m^2 and 72.3% at 3A/m^2, respectively. Furthermore, it also can be seen that the chord length in the control sample is mainly distributed in the range of 0.04-0.22mm with a frequency of 65.9%, and the maximum frequency appears in the chord length range of 0.10-0.12mm. For ECE treated samples, the mainly distributions of the chord length in C1T25, C2T25 and C3T25 are 0.06-0.45mm with a frequency of 80.8%, 0.08-0.50mm with a frequency of 81.0% and 0.08-1.0mm with a frequency of 86.6%, respectively. Correspondingly, the maximum frequencies are appeared in the chord length ranges of 0.16-0.18mm, 0.22-0.24mm and 0.28-0.30mm, respectively.

Fig. 16 (b) shows the distribution of chord length in external concrete (sample Fig. 8(d)). It can be seen that the frequency of the chord length that less than 0.22mm in control sample is 72.2%. As the current density increases, the frequencies of the chord length in this range of samples C1T25, C2T25 and C3T25 are decreased to 64.3%, 48.7% and 49.4%, respectively. The maximum frequency of the chord length range in control sample is 0.12-0.14mm, which are 0.30-0.35mm and 0.28-0.30mm in samples C1T25, C2T25 and C3T25, respectively.

Previous studies have stated that the cathodic reaction products of H_2 may cause the crack of rebar-concrete interfacial zone [39]. What is more, ECE process can result in the decomposition of C-S-H gel, and the decomposition amount increases with the increase in current density [11, 45]. Therefore, ECE changes the pore distribution of concrete and results in the decrease in small pore and the increase in large pore in internal and external concrete with the increase in current density.

Meanwhile, the ranges of chord length with the maximum frequency in concrete are increased after ECE treatment. As a result, the compressive strengths are decreased due to the poor aperture distribution of ECE treated sample. However, existing reports on the pore size evolution affected by ECE are inconsistent. Some studies stated that ECE increased the porosity of the concrete, which was mainly caused by the increase of small pore[52]. Other studies showed that ECE increased the average pore size and resulted in the porosity increased at the innermost while decreased at the outermost layer of concrete [11, 53].

3.5 Efficacy coefficient analysis

In order to more reasonably design the ECE method, efficacy coefficient method is carried to evaluate the chloride removal parameters. Efficacy coefficient method is based on the principle of multi-objective programming. According to the complexity of the evaluation object and calculates a score to object from different aspects, avoiding the error caused by single evaluation. In General, the efficacy coefficient analysis needs to determine the satisfactory value and the disallowed value of each index in the project. The upper limit is determined as the satisfactory value, and the unsatisfied value is determined as the lower limit of the evaluation index. By calculating the satisfaction degree of each index, the score of the index is determined, and then the comprehensive situation of each item in the research object is evaluated through the synthesis of weighted average. The calculation model is shown as Eq. (6) and the values of 40 and 60 are the specified coefficients in the calculation process. After scoring each index in the project and normalizing the efficacy coefficient by Eq. (7), the total efficacy coefficient *D* of the corresponding indicators in each project is obtained.

$$d_i = \frac{x_i - x_i^s}{x_i^h - x_i^s} \times 40 + 60 \qquad (6)$$

$$D_i = \sqrt[n]{\prod_{i=1}^{n} d_i} \qquad (7)$$

where, d_i is the efficacy coefficient of each evaluation index. x_i is the value of index *i*. x_i^s is the minimum value in the project. x_i^h is the maximum value in the project.

In this section, the chloride removal efficiency (*CE*), bonding strength retention (*BR*) [45] and compressive strength retention (*CR*) (strength retention value=1- loss rate of the strength) are analyzed by efficacy coefficient method, as shown in Table 6.

Table 6. Index values and efficacy coefficient

Samples	Index values (%)			Efficacy coefficient			
	CE	*BR*	*CR*	d_1	d_2	d_3	*D*
C1T15	39.9	95.1	89.5	60.0	100.0	73.7	76.2
C2T15	52.5	90.2	87.2	73.1	86.4	64.7	74.2
C3T15	65.2	83.4	86.0	86.2	67.5	60.0	70.4
C1T25	45.1	94.6	91.3	65.4	98.6	80.8	80.5
C2T25	58.9	87.6	89.3	79.7	79.2	72.9	77.2

C3T25	71.9	83.2	88.0	93.2	66.9	67.8	75.1
C1T35	49.4	93.4	96.2	69.8	95.3	100.0	87.3
C2T35	63.4	86.1	94.0	84.4	75.0	91.4	83.3
C3T35	78.5	80.7	91.9	100.0	60.0	83.1	79.3

Table 6 shows that temperature and current density have big influences on the total efficacy coefficient *D* of ECE. When the temperature is the same, the total efficacy coefficient *D* decreases with the increase in current density. While, under the same current density, the value of *D* increases with the increase in temperature. The optimal total efficacy coefficient *D* with the value of 87.3 is achieved with the ECE parameters of $1A/m^2$ and 35℃. However, as abovementioned, when the current density of ECE is $1A/m^2$, the low chloride removal efficiency results in the corrosion of rebar. And a higher current density has a relatively high adverse effect on the mechanical properties of the samples. Therefore, comprehensively consider the influences of these factors, the optimal parameters for ECE are at $2A/m^2$ and 35℃. However, the optimal parameters for ECE were varied due to the not fully considering the effects of ECE on the properties of reinforced concrete. For example, to obtained a relative high ECE efficiency, some studies stated that a higher temperature resulted a larger ECE efficiency, especially at 40℃[20, 21]. Other reports stated that the proper current density for ECE were $0.5A/m^2$ [23] and $3A/m^2$ [54], respectively.

4. CONCLUSIONS

This paper mainly studied the ions distribution, mechanical properties and aperture evolution of reinforced concrete after ECE treatment with varying current densities and temperatures. Main conclusions are drawn as follows:

(1) Current density is the primary factor that affects the chloride extraction efficiency of ECE. The effect of temperature on the improvement of ECE efficiency is limited. When the current density and temperature of ECE are $3A/m^2$ and 35℃, the optimal efficiency of chloride removal is 78.5%.

(2) ECE treatment can significantly decrease the Cl^- content and reduce the corrosion risk of reinforced concrete when at an appropriate current density. After ECE, the Cl^- content nearby rebar reduces significantly and presents an increasing trend from rebar surface to concrete surface. The OH^-, K^+, Na^+ and Ca/Si ratio are increased nearby the rebar region with the increase in current density and are presented a decreasing trend from inside to outside of the concrete.

(3) Although ECE can reduce the corrosion risk of reinforced concrete, it has adverse effects on the compressive strength of concrete due to the decrease of small pore and increase of large pore in concrete after ECE treatment with the increase in current density.

(4) Comprehensively consider the influences of ECE on chloride removal efficiency, bonding strength retention and compressive strength retention by using efficacy coefficient analysis, the optimal parameters for ECE treatment are at $2A/m^2$ and 35℃.

ACKNOWLEDGEMENT
This research was supported by the National Natural Science Foundation of China (52078015 & 51678011).

References

1. X. Shi, N. Xie, K. Fortune and J. Gong, *Constr. Build. Mater.*, 30 (2012) 125.
2. J. Chang, *Cem. Concr. Res.*, 32 (2002) 657.
3. V. Saraswathy and H. W. Song, *Build. Environ.*, 42 (2007) 464.
4. S. Jorge, D. D. Costa and E.N.B.S. Julio, *Eng. Struct.*, 36 (2012) 372.
5. G.T. Parthiban, R. T. Parthiban, V. Ravi, N. Saraswathy and V.S. Palaniswamy, *Corros. Sci.*, 50 (2008) 3329.
6. R. Al-Hammoud, K. Soudki and T.H. Topper, *J. Compos. Constr.*, 15 (2010) 42.
7. D.A. Koleva, Z. Guo, K.V. Breugel and J.H.W. D. Wit, *Mater. Corros.*, 60 (2009) 344.
8. X. Jing and Y. Wu, *Constr. Build. Mater.*, 25 (2011) 2655.
9. Y. Liu and X. Shi, *Corros. Rev.*, 27 (2009) 53.
10. L. Fan, Y. Bao, W. Meng and G. Chen, *Compos. Part B-Eng.*, 165 (2019) 679.
11. J.Y. Hu, S. Li., Y.Y. Lu, H.Y. Zhang and M.Z. Zhang, *Constr. Build. Mater.*, 249 (2020) 118717
12. E.Q. Zhang, Z. Abbas and L. Tang, *Constr. Build. Mater.*, 185 (2018) 57.
13. B. Elsener and U. Angst, *Corros. Sci.*, 49 (2007) 4504.
14. C.C. Chang, W. Yeih and J.J. Chang, *Constr. Build. Mater.*, 68 (2014) 692.
15. R.D.A.S. Luan, M.H.F.D. Medeiros, E. Pereira and A.P.B. Capraro, *Constr. Build. Mater.*, 145 (2017) 435.
16. L.X. Mao, Z. Hu, J. Xia, G.L. Feng, I. Azim, J. Yang and Q.F. Liu, *Compos. Struc.*, 207 (2019) 176.
17. G. Fajardo, G. Escadeillas and G. Arliguie, *Corros. Sci.*, 48 (2006) 110.
18. J.H. Zhu, L.L. Wei, Z.H. Wang, K. Cheng and Y. Fang, *Constr. Build. Mater.*, 120 (2016) 275.
19. U. Ancst, B. Elsener and C.K. Larsen, *Cem. Concr. Res.*, 39 (2009) 1122.
20. T. Ueda, K. Wakitani and A. Nanasawa, *Electrochim. Acta*, 86 (2012) 23.
21. J. Xia, Q.F. Liu, J.H. Mao, Z.H. Qian, S.J. Jin, J.Y. Hu and W.L. Jin, *Constr. Build. Mater.*, 193 (2018) 189.
22. A.M. Hassanein, G.K. Glass and N.R. Buenfeld, *Corrosion-US*, 54 (1998) 323.
23. V. Saraswathy, H.S. Lee, S. Karthick and S.J. Kwon, *Constr. Build. Mater.*, 158 (2018) 549.
24. Z.Q. Jin, D.S. Hou and T.J. Zhao, *Constr. Build. Mater.*, 173 (2018) 149.
25. K.B. Kim, J.P. Hwang and K.Y. Ann, *Constr. Build. Mater.*, 104 (2016) 191.
26. W. Yeih, J.J. Chang, C.C. Chang, K.L. Chen and M.C. Chi, *Cem. Concr. Compos.*, 74 (2016), 136.
27. T.D. Marcotte, C.M. Hansson and B.B. Hope, *Cem. Concr. Res.*, 29 (1999) 1555.
28. M. Siegwart, B.J. McFarland, J.F. Lyness and A.A. Tair, *Corrosion-US*, 58 (2002) 257.
29. Y. Liu and X. Shi, *Constr. Build. Mater.*, 27 (2012) 450.
30. P. Garces, M.J.S.D. Rojas and M.A. Climent, *Corros. Sci.*, 48 (2006) 531.
31. T.H.Y. Nguyen, W. Pansuk and P. Sancharoen, *KSCE J. Civil Eng*. 22 (2018) 2942.
32. H.Y.T. Nguyen, H. Yokota and K. Hashimoto, *J. Adv. Concr. Technol*. 13 (2015) 564.
33. R. Elgebaley, Y. Elshazly and M. Elsalamawy, *Construct. Build. Mater*. 208 (2019) 444.
34. G.E. Abdelaziz, A.M.K. Abdelalim and Y.A. Fawzy, *Cem. Concr. Res*., 39 (2009) 727.
35. Y. Tissier, V. Bouteiller, E.M. Victoire, S. Joiret, T. Chaussadent and Y.Y. Tong, *Electrochim. Acta*, 317 (2019) 486.
36. J.M. Miranda, A. Cobo, E. Otero and J.A. Gonzalez, *Cem. Concr. Res*., 3 (2007) 596.
37. J. Chang, *Constr. Build. Mater.*, 17 (2003) 281.
38. H.Y. Shan, J.X. Xu and Z.Y. Wang, *Constr. Build. Mater.*, 127 (2016) 344.
39. M. Castellote, C. Andrade and M.C. Alonso, *ACI Mater. J.*, 96 (1999) 314.

40. R.N. Swamy and S. Mchugh, *Cem. Concr. Compos.*, 28 (2006) 722.
41. A. Cañón, P. Garcés, M. A. Climent, J. Carmona and E. Zornoza, *Corros. Sci.*, 77 (2013) 128.
42. A. Toumi, R. Francois and O. Alvarado, *Cem. Concr. Res*., 37 (2007) 54.
43. L.Y. Li and C.L. Page, *Comp. Mater. Sci.*, 9 (1998) 303.
44. M. Castellote, C. Andrade and C. Alonso, *Cem. Concr. Res*., 30 (2000) 615.
45. H. Lin, Y. Li and Y.Q. Li, *Constr. Build. Mater.*, 197 (2019) 228.
46. T.Y. Hao, H. Lin and Y. Li. *IOP Conference Series: Mater. Sci. Eng.*, 544 (2019) 012031.
47. D.S. Hou, H.D. Yan and J.R. Zhang, *Constr. Build. Mater.*, 112 (2016) 331.
48. B.W. Xu, H.Y. Ma and Z.J. Li, *Cem. Concr. Res*., 68 (2015) 1.
49. H.Y. Ma, B.W. Xu and J. Liu, *Mater. Design*, 64 (2014) 497.
50. Y. Li, X.F. Liu and M.K. Wu, *Constr. Build. Mater.*, 153 (2017) 436.
51. N.M. Ihekwaba and B.B. Hope, *Cem. Concr. Res*., 26 (1996) 771.
52. M. Siegwart, J.F. Lyness and B.J. McFarland, *Cem. Concr. Res*., 33 (2003) 1211.
53. D. Rodrigo, M.D. Medeiros, E. Pereira and A. Capraro, *Constr. Build. Mater.*, 145 (2017) 435.
54. Q.F. Liu, L.Y. Li, D. Easterbrook and J. Yang, *Eng. Struct.*, 42 (2012) 201.